

Coding RNAs with a non-coding function

Maintenance of open chromatin structure

Maiwen Caudron-Herger,¹ Katharina Müller-Ott,¹ Jan-Philipp Mallm,¹ Caroline Marth,¹ Ute Schmidt,² Katalin Fejes-Tóth³ and Karsten Rippe^{1,*}

¹Research Group Genome Organization & Function; Deutsches Krebsforschungszentrum (DKFZ) and BioQuant; Heidelberg, Germany;

²Research Group Intracellular RNA Trafficking; Institut de Génétique Moléculaire de Montpellier CNRS-UMR 5535; Montpellier, France;

³California Institute of Technology; Pasadena, CA USA

Key words: chromatin organization, heterochromatin, fluorescence microscopy, transcriptome sequencing, nuclear architecture, untranslated RNA regions, microinjection

The multi-layered organization of the genome in a large nucleoprotein complex termed chromatin regulates nuclear functions by establishing subcompartments with distinct DNA-associated activities. Here, we demonstrate that RNA plays an important role in maintaining a decondensed and biologically active interphase chromatin conformation in human and mouse cell lines. As shown by RNase A microinjection and fluorescence microscopy imaging, digestion of single-stranded RNAs induced a distinct micrometer scale chromatin aggregation of these decondensed regions. In contrast, pericentric heterochromatin was more resistant to RNase A treatment. We identified a class of coding RNA transcripts that are responsible for this activity, and thus termed these 'chromatin-interlinking' RNAs or ciRNAs. The initial chromatin distribution could be restored after RNase A treatment with a purified nuclear RNA fraction that was analyzed by high-throughput sequencing. It comprised long >500 nucleotides (nt) RNA polymerase II (RNAP II) transcripts that were spliced, depleted of polyadenylation and was enriched with long 3'-untranslated regions (3'-UTRs) above ~800 nt in length. Furthermore, similar reversible changes of the chromatin conformation and the RNAP II distribution were induced by either RNA depletion or RNAP II inhibition. Based on these results we propose that ciRNAs could act as genome organizing architectural factors of actively transcribed chromatin compartments.

Introduction

Chromatin organization regulates access of the transcription, repair and replication machineries to the DNA at the level of the nucleosome, the folding of the nucleosome chain as well as its higher order architecture in the nucleus.¹⁻⁵ With respect to the structural principles that govern the arrangement of the nucleosome chain during interphase, two types of models have been proposed. In the nuclear matrix model, a proteinaceous fiber network acts as the nuclear equivalent to the cytoskeleton to organize chromatin.⁶⁻⁸ In an alternative view, key determinants of genome structure during interphase are intra- and inter-chromosomal linkages that are tightly interconnected with the gene expression state of a given locus.⁹ This dynamic genome scaffold is established by (i) 'transcription factories' of RNA polymerase II (RNAP II),¹⁰⁻¹² that might be important for RNA 'trans-splicing',¹³ (ii) the nucleolus as a RNA polymerase I transcription organelle,¹⁴ (iii) gene clusters, in which gene dense regions are separated from gene poor regions¹⁵ and (iv) 'active chromatin hubs' between regulatory chromatin elements.¹⁶ This raises the question whether RNA itself is a structural organizer of chromatin. Indeed, several studies have reported on the association of RNA with chromatin and a possible role of RNA in

establishing a nuclear scaffold or other nuclear subcompartments.^{7,17-25} Furthermore, the cell's nuclear architecture shows distinct differences with respect to the biological activity of the corresponding genomic regions as described in detail in a number of reviews.^{2,4,5} Thus, transcription and genome organization are tightly connected from a structural point of view, but also in terms of an interleaved and modular transcriptome.²⁶

Here, we demonstrate that RNA has an important function for maintaining a decondensed and biologically active interphase chromatin conformation. We identified a class of coding RNA transcripts that are responsible for this activity, and thus termed these 'chromatin-interlinking' RNAs or ciRNAs. Based on the similarities between changes of the chromatin conformation and the RNAP II distribution induced by RNA depletion or RNAP II inhibition, we propose that ciRNAs could act as genome organizing cross-linkers of actively transcribed chromatin.

Results

RNA is required to maintain an open chromatin state. To investigate whether RNA is involved in chromatin organization, we microinjected different RNases into the cell nucleus and compared their effects on chromatin distribution to proteinase K,

*Correspondence to: Karsten Rippe; Email: Karsten.Rippe@dkfz.de
Submitted: 06/20/11; Revised: 08/11/11; Accepted: 08/12/11
<http://dx.doi.org/10.4161/nucl.2.5.17736>

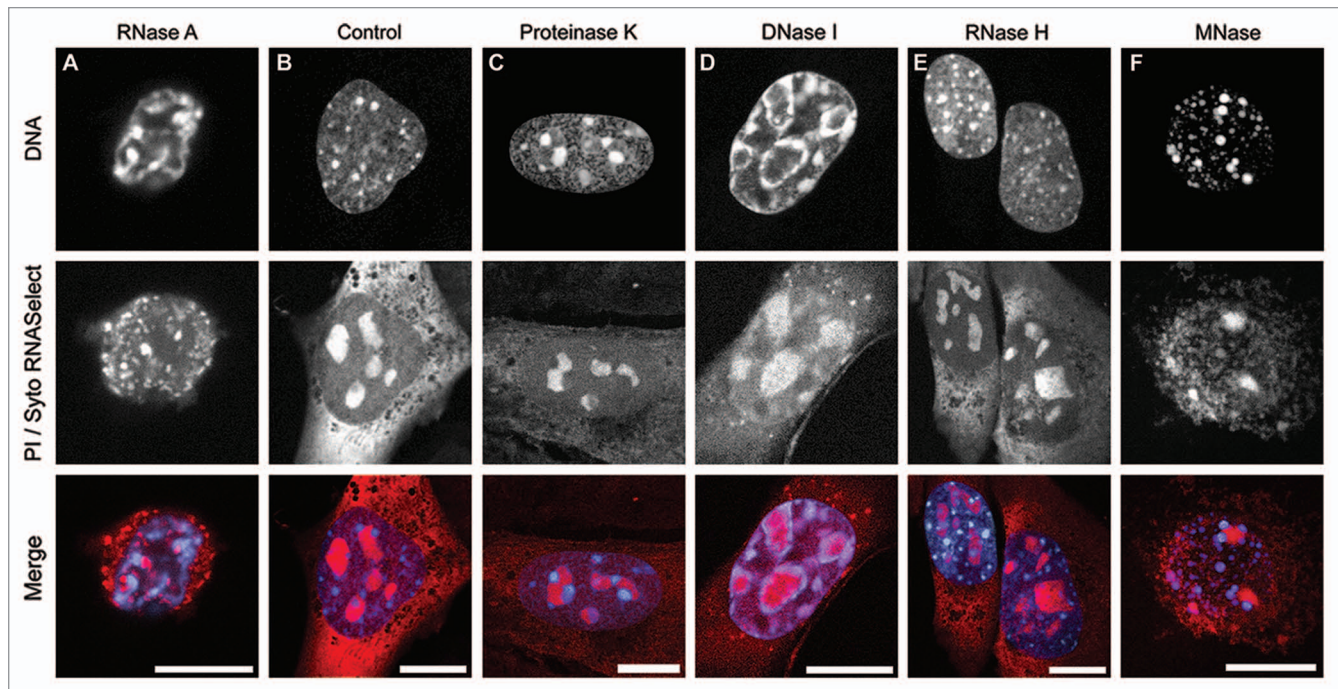


Figure 1. Interphase chromatin distributions after exposure to different enzymatic activities that target RNA, DNA or proteins. (A–E) Confocal laser scanning microscope (CLSM) images of NIH 3T3 mouse fibroblasts microinjected with the indicated enzymes or the corresponding volume of buffer for control samples. Buffer-injected control samples were indistinguishable from each other and only the RNase A control is shown. DNA (blue) was stained with DAPI and RNA via PI (red) or with Syto RNaseSelect for MNase digestion in (F), which was conducted with permeabilized cells. Scale bars, 10 μ m.

DNase I or micrococcal nuclease (MNase) (Fig. 1 and Table S1). First, mouse NIH 3T3 cells were investigated, in which the pericentric heterochromatin localizes to distinct foci (chromocenters) so that euchromatic and heterochromatic regions can be easily distinguished on the microscopy images.^{27,28} Upon microinjection of RNase A into the nucleus, a striking rearrangement of the chromatin distribution with a μ m-scale aggregation of chromatin at the nuclear periphery was observed (Fig. 1A). The propidium iodide (PI) labeling became irregular, and the nucleoli disintegrated while the nuclear lamina remained intact (Fig. S1). No change of nuclear structure was detected upon microinjection of buffer in the control samples.

The effect of RNase A was clearly distinct from proteinase K, DNase I and MNase treatment (Fig. 1 and Table S1). With proteinase K, the PI staining was similar to the control cells (Fig. 1B and C). However, large chromatin aggregates formed mostly around the nucleoli and at the nuclear periphery within a heterogeneous chromatin fiber network. Microinjecting DNase I led to condensed chromatin that localized to the nuclear periphery and around the nucleoli. Aggregates of different sizes formed, which were connected via weakly labeled chromatin tracts. Various restriction enzymes had no effect (Table S1). Upon MNase digestion, the chromatin organized into numerous round $\sim 1 \mu$ m aggregates (Fig. 1F). The changes induced to the structure of the nucleolus were less significant than with RNase A.

The effect of RNase A was also investigated in human HeLa and MCF-7 cell lines where denser heterochromatin regions are small in size. In these the induction of chromatin aggregation can be clearly distinguished from pre-existing heterochromatin loci.

RNase A treatment of human cell lines led to the same drastic chromatin compaction that was observed with mouse NIH 3T3 cells. This indicates that the requirement of RNA for maintaining an open chromatin state is a general feature of mammalian cells (Fig. 2).

In order to confirm that the observed collapse of chromatin structure was a direct effect of the degradation of structurally important RNAs, we conducted time course experiments in living cells. The chromatin distribution was imaged in HeLa cells just after microinjection of RNase A (Fig. 3) via a YFP-fused histone H2A marker. RNase A treatment did not induce histone dissociation from the DNA as apparent from the persistent colocalization of histone H2A-YFP fluorescence and DAPI signal. The effect of RNA digestion on chromatin organization started within 1 minute after microinjection and is clearly seen after 5 min on the fluorescence intensity profile (Fig. 3): The fluorescence intensity in the control-injected cells showed some variations that reflect the differences in chromatin compaction in HeLa cells that have been evaluated in detail previously in reference 29 and 30. This fluorescence intensity distribution became much more heterogeneous in the RNase A-injected cells and revealed the aggregation of chromatin domains on the micrometer length scale. A longer RNase A treatment was studied by fixing NIH 3T3 cells immediately, 20 to 50 min and 150 to 180 min after injection (Fig. S2). Shortly after microinjection, the chromatin distribution changed and the maximum effect was reached after 20 min incubation. In contrast, induction of apoptosis required about 90 min and occurred clearly after the chromatin reorganization event (Fig. S3). At 150 to

180 minutes the buffer-injected cells displayed no effect on chromatin, and this was true for at least 24 hours without affecting cell viability. However, almost all RNase A-injected cells had died and detached from the surface after that time. These results confirm that the chromatin re-organization following the injection of RNase A is a process that does occur on the minute scale and is not due to induction of apoptosis.

Single-stranded RNAs are essential for chromatin structure organization. Some features of the RNAs involved in the structural maintenance of chromatin could be inferred from comparing the effect of RNase A to other microinjected RNases. RNase A preferentially cleaves single-stranded RNA, RNase III and RNase VI degrade double-stranded RNA and RNase H cleaves RNA in a DNA-RNA hybrid (Table S1). In addition, we tested cleavage of short RNA oligoribonucleotides (<7 nt) by the Orn oligoribonuclease.³¹ None of these RNases could reproduce the chromatin distribution pattern observed after RNase A injection (Fig. 1A and Table S1). With RNase H, the chromatin organization hardly changed (Fig. 1E), indicating that DNA-RNA hybrids are less important in higher-order chromatin organization. We conclude that the activity of RNA to maintain an open chromatin conformation involves single-stranded RNA linkages.

Heterochromatin structure is less sensitive to RNA digestion than euchromatin. An investigation of the heterochromatin markers histone H3 trimethylation at lysine 9 (H3K9me3), the proteins HP1 α and Suv39h1 revealed that the integrity of pericentric heterochromatin was partially maintained after RNase A treatment (Fig. 4). In mouse cells, H3K9me3, Suv39h1 and HP1 α accumulate in distinct DAPI dense foci of pericentric heterochromatin referred to as chromocenters. These can be easily distinguished from the less dense euchromatic regions in the fluorescence microscopy analysis.^{27,28} This was exploited in the experiments shown in Figure 4 to evaluate differences between eu- and heterochromatin in response to RNase A treatment (Fig. 4A) in comparison to the effect of DNase I (Fig. 4C) and MNase (Fig. 4D). The results show that RNase A digestion had a strongly reduced effect on heterochromatin structure as compared to euchromatin. As reported previously, HP1 α became dispersed, which is indicative of the participation of an RNA component in its interaction with the chromocenters.^{27,32} In contrast, two other markers of pericentric heterochromatin in mouse cells, Suv39h1 and H3K9me3, remained associated at the chromocenters upon microinjection of RNase A. The H3K9me3 modification is stably attached to pericentric heterochromatin and a good marker for preservation of its compaction state. It became more dispersed in the nucleus only after DNA digestion by DNase I and MNase (Fig. 4C and D). Thus, apart from the RNA-dependent binding of HP1 α , the heterochromatic chromocenters were mostly resistant towards RNase A treatment. This indicates that the structural requirements of chromatin for RNA were more pronounced in euchromatin than in heterochromatin regions.

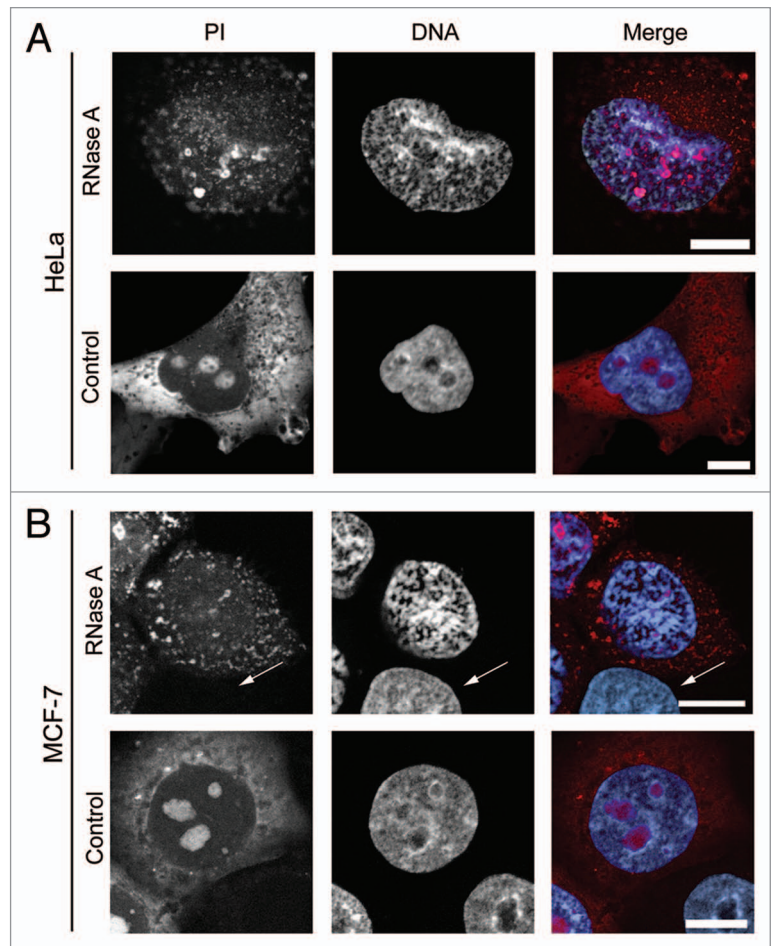


Figure 2. Chromatin aggregation in human HeLa and MCF-7 cells after RNase A microinjection. CLSM images of (A) HeLa and (B) MCF-7 cells after microinjection. The arrow in (B) indicates a non-injected cell. Note the similarity in the chromatin distribution with the control cell (buffer injection) in the picture below. The injection mix contained propidium iodid (red) and either RNase A or the corresponding volume of RNase A buffer as control. DNA was stained with DAPI (blue). Scale bars, 10 μ m.

Chromatin-interlinking RNAs (ciRNAs) are enriched in a soluble nuclear RNA fraction. To further characterize the RNAs responsible for maintaining the native chromatin distribution, we investigated the ability of different RNA fractions to rescue the chromatin collapse after RNase A treatment in permeabilized HeLa cells. This is an alternative method to expose chromatin to RNase A, and yielded results very similar to the RNase A microinjection experiments. The assay consisted of RNase A treatment and subsequent addition of RNase inhibitor and different amounts of various types of RNA to evaluate their propensity to rescue the initial chromatin distribution (Fig. 5A). It is noted that the dissolution of the nucleoli could not be reversed in this manner under the conditions tested. The RNase A-induced changes of chromatin organization and their reversal could be clearly identified visually by following the changes in the fluorescence intensity distribution of the DAPI signal. In addition, these differences were also quantitated via computing the fractal dimension of the nuclear DAPI staining

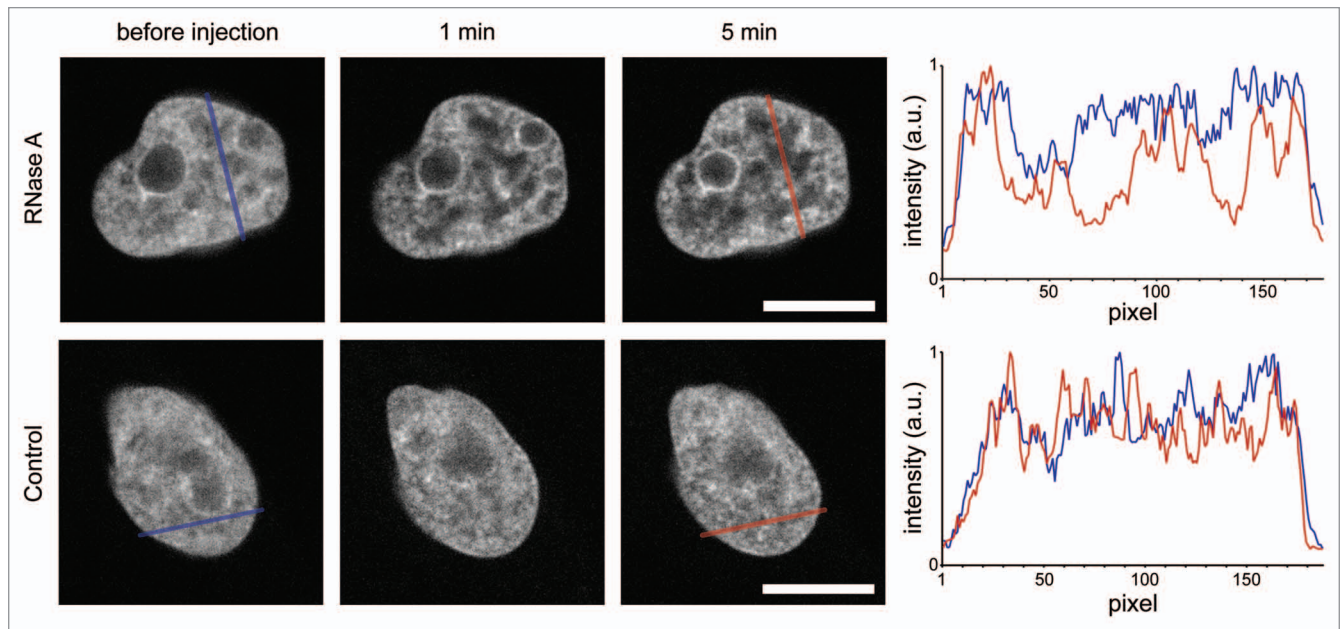


Figure 3. Chromatin aggregation kinetics after RNase A microinjection in living cells. Chromatin reorganization and aggregation in HeLa cells as monitored via H2A-YFP fluorescence occurred immediately after RNase A microinjection. This is readily apparent from the changes of the fluorescence intensity profile before (blue line) versus 5 min after (red line) microinjection. No such changes were observed in the control cells upon buffer microinjection. Scale bars, 10 μm .

as shown in **Figure 5B** as an unbiased parameter that describes the granularity of the chromatin distribution.²⁹ According to our analysis a fraction of $75 \pm 2\%$ of the RNase A-treated cells displayed an aggregated chromatin structure as opposed to only $19 \pm 2\%$ of the control cells.

We used this rescue assay to systematically test RNA fractions that were obtained from HeLa S3 cells according to the scheme depicted in **Figure 6A**. It yielded total RNA, cytoplasmic RNA and nuclear RNA. The latter was further separated into a soluble nuclear extract from which four RNA fractions F1 to F4 were obtained after a sucrose gradient purification, as well as RNAs stably associated with soluble chromatin fragments and a nuclear pellet (**Fig. 6** and Materials and Methods). These RNAs and a number of others were evaluated in the rescue assay (**Fig. 7A**). The addition of total RNA to the RNase A-treated cells at a concentration of 70 $\text{ng}/\mu\text{l}$ led to an almost complete recovery with respect to the chromatin distribution. However, a lower concentration of 10 $\text{ng}/\mu\text{l}$ did not rescue the chromatin structure when the following RNAs were added: total RNA, nuclear pellet, homopolymeric poly(A) RNA, tRNA and rRNA. The cytoplasmic, nuclear and chromatin RNA fractions had only a small effect with respect to restoring an open chromatin conformation (**Fig. 7A**). The F2 RNA fraction contained 500 to 2,000 nt long RNAs and displayed the highest activity (**Figs. 6C** and **7A**). It was able to fully reverse the RNase A-induced chromatin condensation at 10 $\text{ng}/\mu\text{l}$ concentration and induced a significantly better recovery than any other fraction even at 3 $\text{ng}/\mu\text{l}$. We concluded that the activity of RNA to maintain an open chromatin conformation was restricted to a specific class of single-stranded RNAs, which we termed ‘chromatin-interlinking’ RNAs or ciRNAs. These are enriched in the F2 RNA fraction.

ciRNAs are nuclear-retained RNAP II transcripts. To determine sequence features of ciRNAs, we compared the F2 RNA, soluble nuclear extract, nuclear RNA, chromatin and total RNA fractions by deep sequencing for two independent preparations. While the overall amount of intergenic RNAs, RNAP II primary transcripts and spliced RNAs was similar (**Table 1**; Materials and Methods), a higher abundance of spliced transcripts was observed in the F2 RNA fraction. A more detailed analysis revealed that the F2 RNA fraction was significantly enriched in spliced transcripts with long 3'-UTR sequences (**Tables 1** and **S2** and **Fig. 7B** and **C**). The most enriched clusters in the F2 RNA fraction were compared to those in the total RNA fraction as described in Materials and Methods. In the F2 fraction $56 \pm 5\%$ of these clusters were overlapping with 3'-UTR regions longer than approximately 800 nt, whereas these represented only $23 \pm 12\%$ in the total RNA sample (**Table S2**). These findings support the model of a structural role of a whole class of RNAs as opposed to a few specific transcripts, that have functional sequence elements encoded in the 3'-UTR.³³ The F2 RNA fraction was depleted of polyadenylated transcripts, which could hinder nuclear export.³⁴ This conclusion is based on (i) the low abundance of polyadenylated RNAs in this fraction when isolating them by oligo T affinity purification, (ii) the persistence of a reconstituting activity in the F2 RNA fraction after depletion of polyadenylated RNAs (**Fig. 7A**), and (iii) an amount of $A_{>20}/T_{>20}$ sequence reads that was only about half of that of the total RNA sample.

RNAs maintain the structural integrity of RNAP II transcription factories. We compared the effect of RNase A with the inhibition of RNAP II by α -amanitin for 4 h. This process was monitored via 5-bromouridine 5'-triphosphate (BrUTP) labeling of nascent RNA. In both HeLa and NIH 3T3 cells, the native

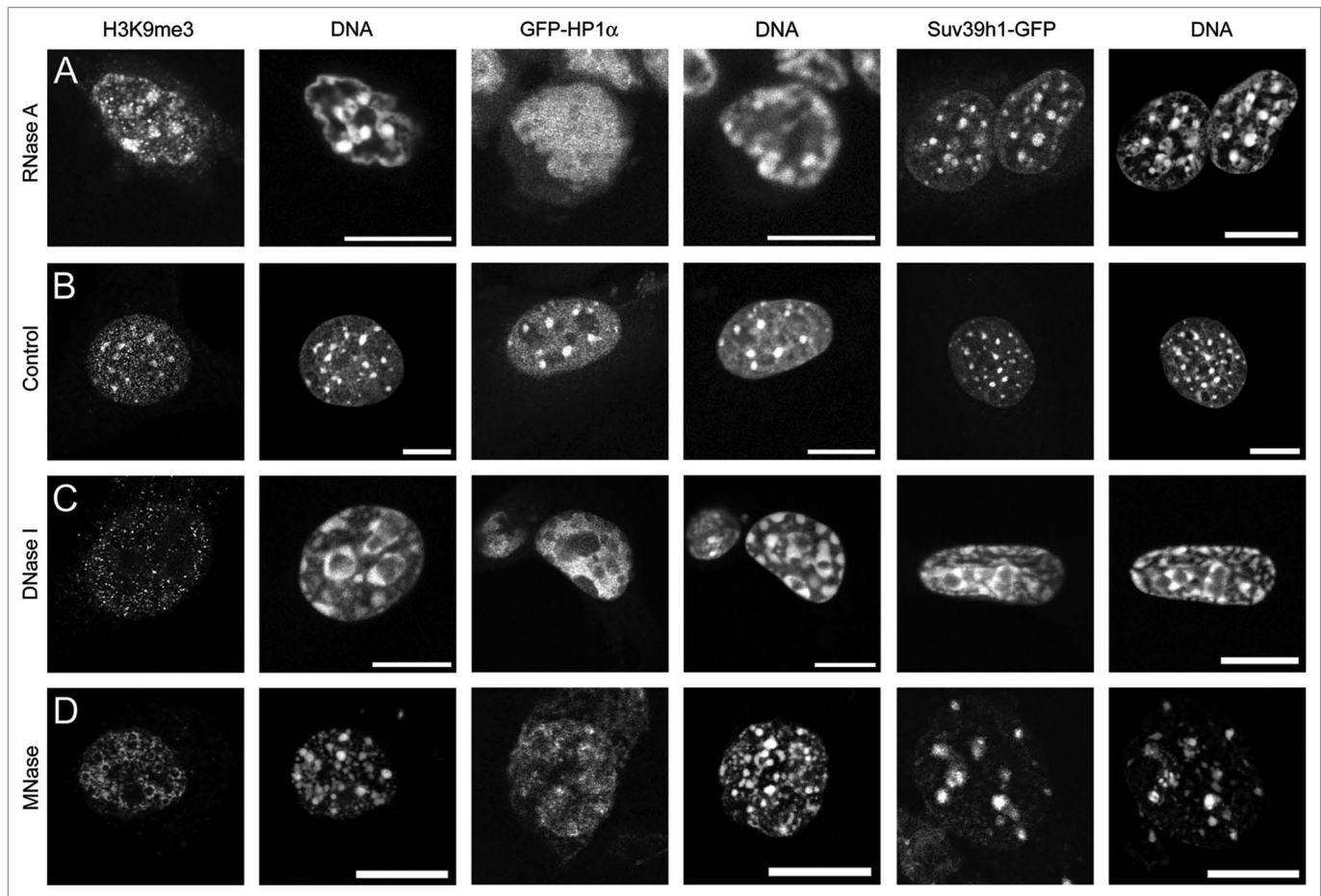


Figure 4. Effect of RNase A digestion on heterochromatin versus euchromatin. Three markers of pericentric heterochromatin in mouse NIH 3T3 cells, H3K9me3 visualized by immunofluorescence (IF) as well as Suv39h1-GFP and GFP-HP1 α were evaluated. DNA was stained with DAPI. Scale bars, 10 μ m. (A) RNase A microinjection. (B) Control. (C) DNase I microinjection. (D) MNase added to permeabilized cells.

punctuated nuclear BrUTP-labelled RNA distribution disappeared in the presence of α -amanitin. The chromatin became porous and partially aggregated (Fig. 8A and B). The nucleoli fragmented into a beads on a string-like structure as reported previously in reference 35 and 36. Thus, the two main effects of RNase A, namely the aggregation of chromatin and the resolution of nucleoli, were also present when RNAP II was inhibited, albeit to a lower degree. This supports the conclusion that ciRNAs are synthesized by RNAP II. The addition of the translation inhibitor cycloheximide had no effect on chromatin distribution, which argues against an aberrant chromatin organization resulting from a lack of protein expression. The function of the ciRNAs in chromatin structure maintenance was independent of active RNAP II, since including α -amanitin in the reaction after RNase A treatment did not prevent the re-establishment of the original decondensed chromatin state by ciRNAs (Fig. 7A).

A chromatin linkage function has been assigned to transcription factories of RNAP II complexes associated with DNA loops, and various lines of evidence have led to the conclusion that these exert a genome organizing function.¹⁰ We reasoned that the structural integrity of transcription factories could require an RNA component. When inducing the disruption of RNAP II

transcription factories by cleaving their DNA component by DNase I or MNase treatment, the initially punctuated RNAP II distribution was transformed into much larger aggregates (Fig. 8C). Notably, a similar pattern was obtained after RNase A microinjection as well as after α -amanitin treatment (Fig. 8C).³⁷ Upon addition of the F2 RNA fraction at a concentration of 10 ng/ μ l the initial dotted distribution of RNAP II was restored (Fig. 9). This correlation points to a possible function of ciRNAs as a structural component of transcription factories.

Discussion

In the present study we report on the drastic genome reorganization that occurs upon digestion of single-stranded RNAs in the nucleus. By combining fluorescence microscopy and microinjection experiments with high-throughput RNA sequencing, a novel structural function of RNA for interphase chromatin organization was characterized and assigned to a class of transcripts termed ciRNAs.

The conformational change observed upon depleting these RNAs could be rescued with a purified nuclear RNA fraction (F2). According to the sequence analysis of this fraction, ciRNAs

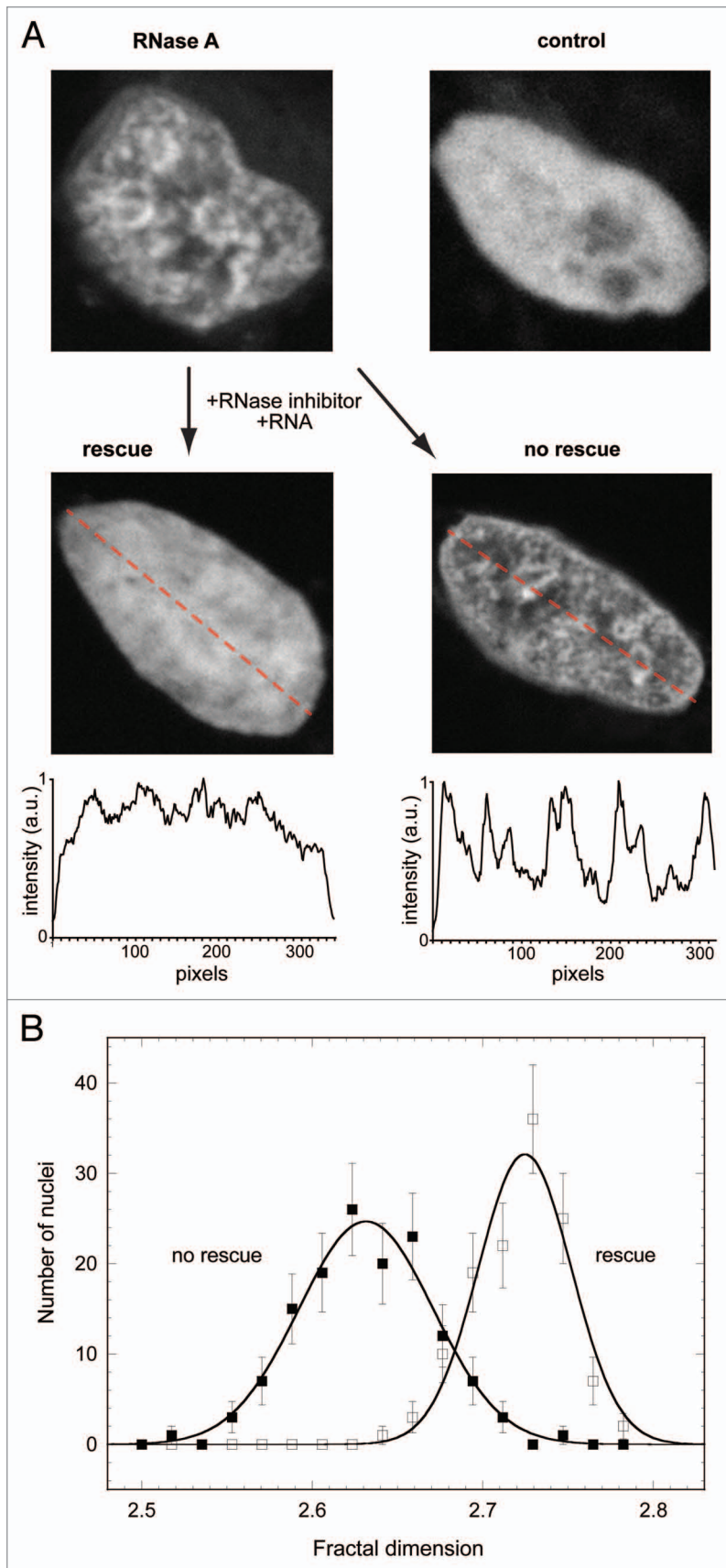


Figure 5. RNA rescue experiments of RNase A-treated permeabilized HeLa cells. (A) The top part shows DAPI stained RNase A-treated and control cells. After RNase treatment, RNase inhibitor and a given RNA fraction were added and incubated 15 min to assess the potential to rescue the initial more homogenous chromatin distribution. The bottom part displays examples for a rescued versus not rescued cell. The intensity profiles along the indicated lines clearly show that the non-rescued cells retained a much more heterogeneous chromatin distribution established after RNase A digestion. (B) Fractal dimension analysis of chromatin distribution in RNase A treated cells and in control cells. As described in Materials and Methods, cells with nuclei classified as intact chromatin (open squares) or aggregated chromatin (solid squares) were subjected to the fractal dimension analysis. The lines are the respective fits using a single species Gaussian function yielding average values and standard deviations of 2.63 ± 0.04 and 2.72 ± 0.03 . The two populations are well separated with an overlap of only about 10%, demonstrating that the two types of chromatin morphology could be reliably distinguished in our analysis. Error bars represent the standard deviation.

originate from mostly long (>500 nt) RNAP II transcripts that are subject to splicing. They have reduced polyadenylation, which could impede their nuclear export.³⁴ Their long 3'-UTRs may contain sequence elements that are needed for interlinking chromatin domains. This is in line with the view that 3'-UTRs contain a number of interaction motifs that are encoded in their sequence or secondary structure.³³ As inferred from the size distribution of the purified F2 fraction (Fig. 6C) in comparison with the corresponding genes and 3'-UTRs (Fig. 7C), it is concluded that a significant part of the RNAs in our preparation are not full-length transcripts with the complete 3'-UTR. This might be due to endogenous RNA processing or cleavage during the purification. In this context it is noteworthy that a recent report describes the separate expression of a large number of 3'-UTRs in human and mouse cells.⁵⁴ These are likely to be generated by post-transcriptional cleavage of the corresponding protein-coding sequences. The ciRNA-containing fraction was extracted from the nuclei with a low salt buffer. Accordingly, it represents a fraction of nuclear RNA that is different from the RNA components reported as part of the nuclear matrix since these remain stably attached to the nuclear pellet during buffer extraction.^{7,20} Similarly, they do not remain associated with purified chromatin fragments as reported for yet another fraction of nuclear RNAs^{21,24} that were also included in our analysis.

The ciRNAs are instrumental to prevent a collapse of interphase euchromatin and serve to maintain its open and transcriptionally active state. This is concluded from our finding that RNase A microinjection had a strongly reduced effect on pericentric

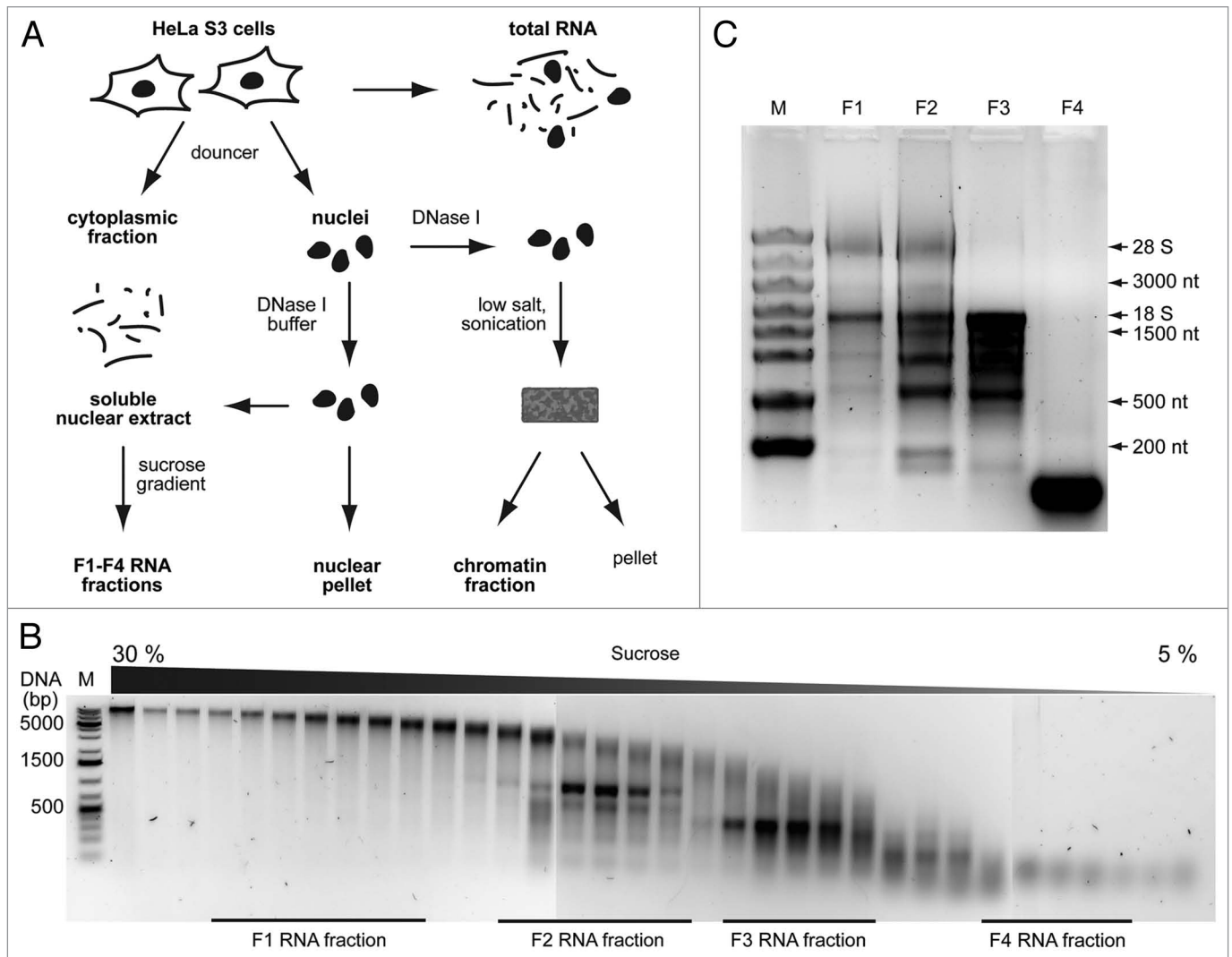


Figure 6. RNA purification procedure. (A) Scheme illustrating the preparation of the different RNA fractions from HeLa S3 cells (see also Materials and Methods). (B) Analysis of RNA fractions on a 12% polyacrylamide gel showing the size gradient of soluble nuclear extract purified from HeLa cell nuclei and centrifuged through a 5–30% sucrose gradient. Selected fractions were pooled to yield the indicated F1, F2, F3 and F4 RNA fractions. The first lane is the DNA marker (M). (C) Electrophoretic analysis of the F1, F2, F3 and F4 RNA fractions on a 1.2% denaturing agarose gel. The first line is a single-stranded RNA marker (M, in nucleotides, nt).

heterochromatin foci in the mouse NIH 3T3 cell line as compared to bona fide euchromatin regions. As reported previously in experiments with permeabilized cells, HP1 α partially dissociated from these regions when RNase A was added, but the DAPI staining indicated that the structural integrity of the chromocenters was mostly retained (Fig. 4).²⁷ In contrast to the loss of the H3K9me2 histone methylation reported in the previous study, we did not observe a significant influence on the presence of H3K9 trimethylation. Both H3K9me2 and H3K9me3 are characteristic features of pericentric heterochromatin, and the observed differences might be related to the experimental conditions (e.g., permeabilization versus microinjection). Our results lead to the conclusion that heterochromatin is mostly resistant to RNase A treatment apart from a partial dissociation of HP1 since three markers of pericentric heterochromatin in mouse, namely intense DAPI staining, H3K9me3 and Suv39h1

persisted. In contrast, the more decondensed euchromatin regions were severely affected and collapsed. An additional line of evidence that relates ciRNAs to active transcription sites comes from the disruption and re-establishment of RNAP II transcription factories upon depletion of RNA with RNase A and subsequent addition of ciRNAs (Figs. 8 and 9).

The change in the observed chromatin compaction pattern induced by RNase A bears some striking similarities to that observed upon ATP depletion^{38–40} or by incubating the cells in a higher ionic strength medium.⁴¹ While ATP depletion could have a similar direct effect as the inhibition of RNAP II by α -amanitin, the chromatin compaction induced via changes of the salt concentration has been explained with a general macromolecular crowding effect.⁴² Furthermore, an increased degree of histone acetylation leads to μ m-scale rearrangements of the chromatin compaction state as well.^{29,30,40} Thus, similar

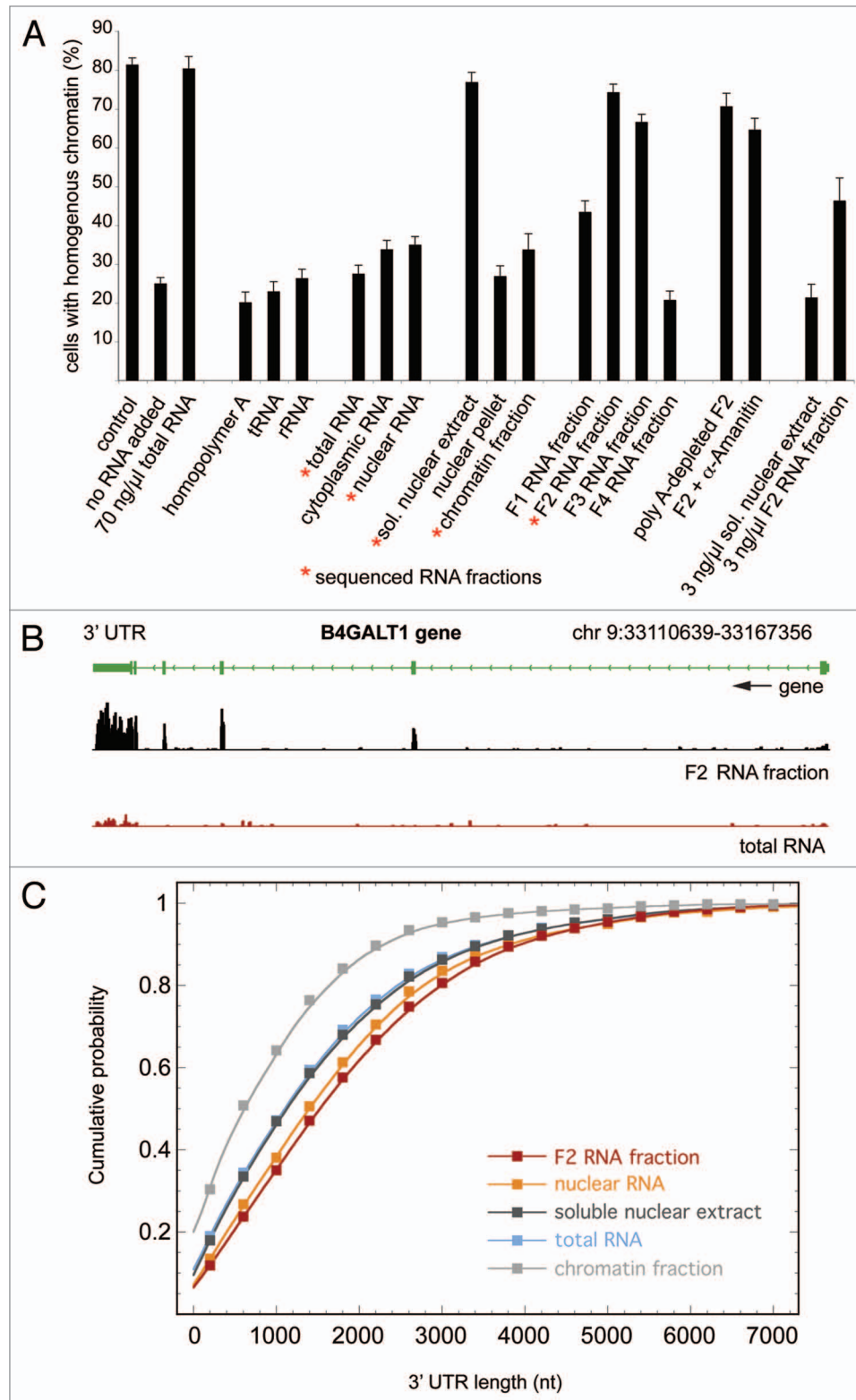


Figure 7. Analysis of RNA fractions in rescue experiments and by deep sequencing. (A) Percentage of cells in which addition of the indicated RNAs (to a concentration of 10 ng/μl unless noted otherwise) rescued the initial homogeneous chromatin after RNase A treatment. Samples of the F2 RNA fraction included the depletion of polyadenylated RNA ("poly A-depleted F2") or addition together with α-amanitin (F2 + α-amanitin). RNAs analyzed by high throughput RNA sequencing are marked with a red star; "sol." stands for soluble. Error bars are the standard deviation for a Poisson distribution. (B) Distribution of the reads from the F2 (black) and total (red) RNA fractions within the B4GALT1 gene (exons, large green rectangles; introns, thin green line). (C) Cumulative probability distribution of 3'-UTR length in the different RNA fractions. A comparison of the distributions reveals an enrichment of the F2 RNA fraction in long 3'-UTR. The maximal difference to the other distributions is at about 1,200 nt length with a p-value < 0.005 according to a Kolmogorov-Smirnov test. Error bars are smaller than the size of the symbols.

Table 1. Distribution of genomic regions in the different RNA fractions

	Genomic regions ^a	Total RNA (%)	Nuclear RNA (%)	Soluble nuclear extract (%)	F2 RNA fraction (%)	Chromatin fraction (%)
Transcripts	intergenic	7 ± 2	10 ± 6	6 ± 2	8 ± 3	9 ± 1
	primary transcripts (exon + intron)	68 ± 6	69 ± 4	74 ± 12	54 ± 8	65 ± 2
	spliced transcripts (exon only)	25 ± 9	22 ± 10	21 ± 14	38 ± 9	24 ± 3
Cluster analysis	TSS	37 ± 3	35 ± 3	35 ± 9	37 ± 1	46 ± 1
	CAGE	13 ± 1	12 ± 1	14 ± 1	13 ± 1	12 ± 2
	promoter	25 ± 1	23 ± 1	22 ± 3	24 ± 1	36 ± 1
	pasRNA	6 ± 2	4 ± 1	4 ± 3	4 ± 1	18 ± 1
	exon	25 ± 10	20 ± 9	21 ± 14	38 ± 10	24 ± 1
	intron	2 ± 1	5 ± 3	1 ± 1	2 ± 1	7 ± 1
	exon-intron overlapping	72 ± 10	73 ± 5	78 ± 14	60 ± 10	62 ± 3
	3'-UTR	34 ± 6	28 ± 8	31 ± 3	41 ± 5	32 ± 2
	intergenic	2 ± 1	2 ± 1	1 ± 1	2 ± 1	7 ± 1
	snoRNAs	2 ± 1	2 ± 1	1 ± 1	2 ± 1	11 ± 1
	tRNAs	0 ± 0	0 ± 0	0 ± 0	0 ± 0	0 ± 1
	miRNAs	0 ± 0	0 ± 0	0 ± 0	0 ± 0	1 ± 1
	rasRNA	3 ± 1	2 ± 1	2 ± 1	3 ± 2	11 ± 1
	repeats	1 ± 1	1 ± 1	3 ± 1	1 ± 1	1 ± 1

^aThe number of transcripts included in the analysis from two independent data sets was 2,344 and 2,141 (total RNA), 2,311 and 1,832 (nuclear RNA), 2,128 and 3,808 (soluble nuclear extract), 1,587 and 5,046 (F2 RNA fraction) and 725 and 535 (chromatin fraction). The cluster distribution was derived from the analysis of 4,463 and 3,049 (total RNA), 4,869 and 2,642 (nuclear RNA), 5,127 and 4,577 (soluble nuclear extract), 3056 and 9643 (F2 RNA fraction) and 1,070 and 679 (chromatin fraction) clusters. Since cluster from different genomic regions are partially overlapping, the sum of all cluster percentages amounts to more than 100%.

structural changes of the nuclear chromatin density distribution can be induced by very different triggers. The normal variations in chromatin compaction throughout the nucleus that are apparent in the CLSM images of human or mouse cell lines have been characterized at higher resolution by electron microscopy imaging⁴³ and structured illumination microscopy.⁴ This led to a model in which more dense chromatin domains are surrounded by a loosely packed biologically active perichromatin compartment (PC) that extends into regions with a largely reduced DNA concentration.⁴⁴ We speculate that the above-mentioned large-scale structural changes preferentially affect the “open” and biologically active PC enriched in transcription sites that surround domains with higher chromatin density. As a result of RNA degradation, increased osmolarity in the medium, ATP depletion or reduced histone acetylation, chromatin that extends into this regions could collapse and associate with the more densely packed chromatin domains.

Accordingly, we propose here that ciRNAs maintain the organization of the PC as depicted in **Figure 10**. In this scheme, four types of mutually non-exclusive mechanisms are considered that would affect the integrity of the open chromatin/PC region. (i) ciRNAs represent a structural component of RNAP II transcription factories and stabilize these entities so that they can act as genome organizers as proposed previously in reference 10–12. (ii) ciRNAs are produced by RNAP II but assemble into chromatin cross-linkers that stabilize interactions between perichromatin fibrils independently of RNAP II. (iii) The PC topology is affected indirectly by ciRNAs via regulating the histone

acetylation state^{29,30,40} or other chromatin-related modifications that change chromatin structure.⁴⁵ (iv) Protein binding of ciRNAs could prevent chromatin association of a protein that would induce chromatin compaction.

All four mechanisms would be compatible with the experimental findings reported here. However, we favor the first hypothetical model depicted in **Figure 10A**, in which ciRNAs act as genome organizing cross-linkers of the PC by stabilizing transcription factories, due to the following considerations: (i) Several lines of evidence argue for a function of transcription factories as genome organizers.^{10–12} (ii) The disruption and re-establishment of RNAP II transcription factories upon depletion of RNA with RNase A and subsequent rescue with ciRNAs correlates with the changes in the chromatin compaction state (**Figs. 8 and 9**). (iii) The RNA sequence analysis in combination with the RNA rescue experiments suggests that spliced coding RNA transcripts with long 3'-UTRs are active in our assay rather than stably chromatin-bound (non-coding) RNAs. Thus, ciRNAs could directly act at the site of their production as a positive feedback signal to maintain the state of active transcription. In contrast mechanisms 2, 3 and 4 in **Figure 10A** would require additional signals for their targeting to transcriptionally active regions. (iv) The RNA mediated histone or DNA modifications according to mechanism 3 appear to be dependent on stably chromatin bound RNAs that are inactive in our assay.^{46–48} Additionally, the rapid collapse and rescue of the chromatin structure argues against recruitment of chromatin modifying enzymes. (v) An RNA-dependent sequestering of a protein involved in chromatin compaction as depicted

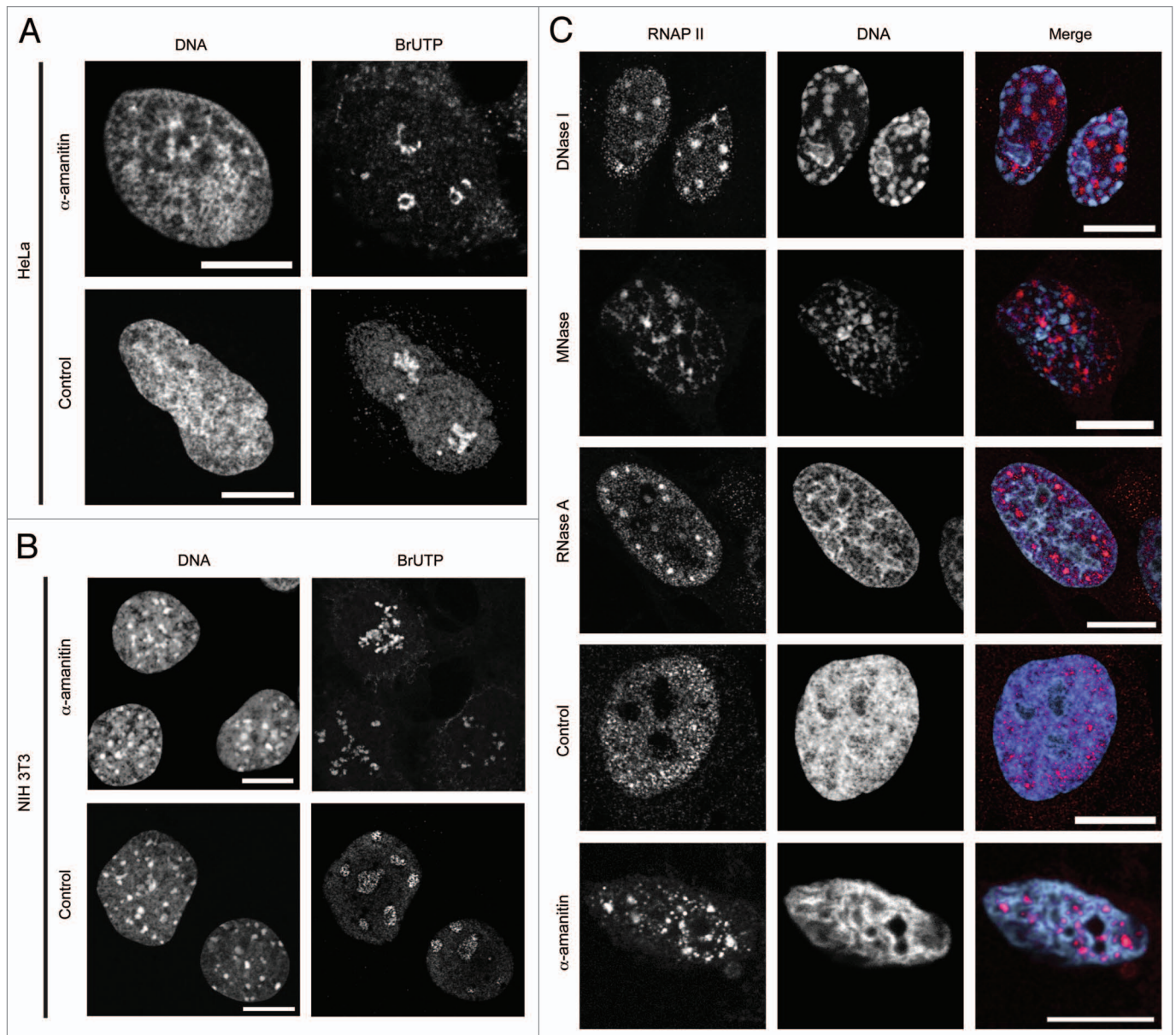


Figure 8. DNA and RNAP II distribution after α -amanitin, DNase I, MNase and RNase A. CLSM images of HeLa (A) and NIH 3T3 cells (B) treated as indicated. DNA was stained with DAPI (blue). BrUTP and RNAP II (red) were visualized by immunofluorescence. (C) IF staining of HeLa cells, injected (DNase I, RNase A), permeabilized (MNase) or treated with α -amanitin, using an anti-RNAP II antibody. Scale bars, 10 μ m.

in mechanism 4 has so far not been reported. Only the opposite process, i.e., the RNA-dependent recruitment of a chromosomal protein has been described, e.g., for HP1 (Fig. 4),^{27,32} or the polycomb repressive complex PRC2.⁴⁹

Clearly, the models discussed above make a number of predictions that require further experiments to corroborate one or the other. For example, we anticipate that the comparative localization of different fluorescently labeled RNAs with respect to active RNAP II will be particularly informative to address the question whether ciRNAs are indeed a component of transcription factories. In addition, chromosome painting in concert with RNase A treatment would allow to identify the subfraction of the PC that is located in between chromosome territories.

This would serve to further delineate the nuclear topology of chromatin domains that require RNA for maintaining their structural integrity. Furthermore, applying the recent advances in fluorescence microscopy imaging of nuclear subcompartments^{4,50} to studies of the RNA-dependent organization of the genome would provide further details on the underlying nuclear architecture.

While the reports on RNA with a putative chromatin organizing function date back to the 1960s and 1970s,¹⁷⁻¹⁹ progress in the field has been hampered by the inability to identify the sequences of the involved RNAs, and to investigate the structural effects of RNA under conditions that preserve the native state of chromatin. Taking stock of nuclear RNAs by sequencing is now becoming

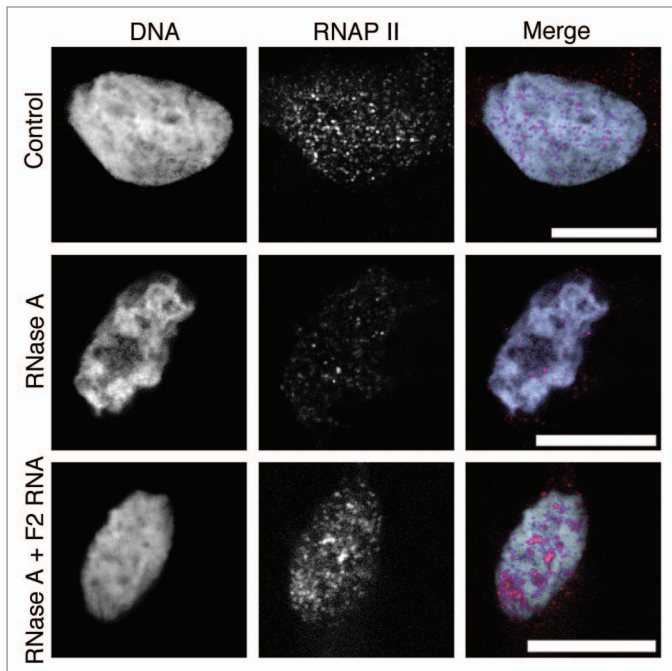


Figure 9. Rescue of RNase A-induced disruption of a punctate RNAP II distribution by addition of the F2 RNA fraction. The RNAP II distribution (red), disrupted by RNase A digestion could be rescued by addition of the F2 RNA fraction at a concentration of 10 ng/ μ l. DNA was stained with DAPI (blue). Scale bars, 10 μ m.

a routine task. However, elucidating their functions requires a phenotype that is frequently not well defined or restricted to tests of a very limited subset of the sequences identified. The combination of fluorescence microscopy imaging, microinjection, RNA fractionation, phenotype rescue experiments and deep sequencing analysis introduced here makes it possible to derive a more comprehensive picture of RNAs as nuclear organizers. Without doubt, a large variety of different pathways exist by which RNAs exert this function as discussed in the context of **Figure 10**. Thus, it will be exciting to further elucidate the network of RNAs that operate in the nucleus to organize the genome into subcompartments that differ in their biological activity.

Materials and Methods

Cell culture. HeLa cells were grown in RPMI 1640 containing 10% FCS, 2 mM L-glutamine and 1% penicillin/streptomycin. NIH 3T3 mouse fibroblasts, wild type or expressing GFP-HP1 α or Suv39h1-GFP, were cultured in Dulbecco's MEM containing 10% FCS, 4.5 g/L glucose, 2 mM L-glutamine and 1% penicillin/streptomycin. MCF-7 were grown in Dulbecco's MEM containing 10% FCS, 2 mM L-glutamine, 1% non-essential amino acids and 1% penicillin/streptomycin. All cell lines were incubated at 37°C at 5% CO₂. For expressing autofluorescent constructs (HeLa, H2A-YFP; NIH 3T3, GFP-HP1 α or Suv39 h1-GFP;²⁸ MCF-7, Bax-GFP⁵¹) growth conditions were the same as those used for the corresponding parental cell lines. For inhibition of RNAP II, cells were grown 4 hrs in medium containing 50 μ g/ml α -amanitin (Sigma). When used in the

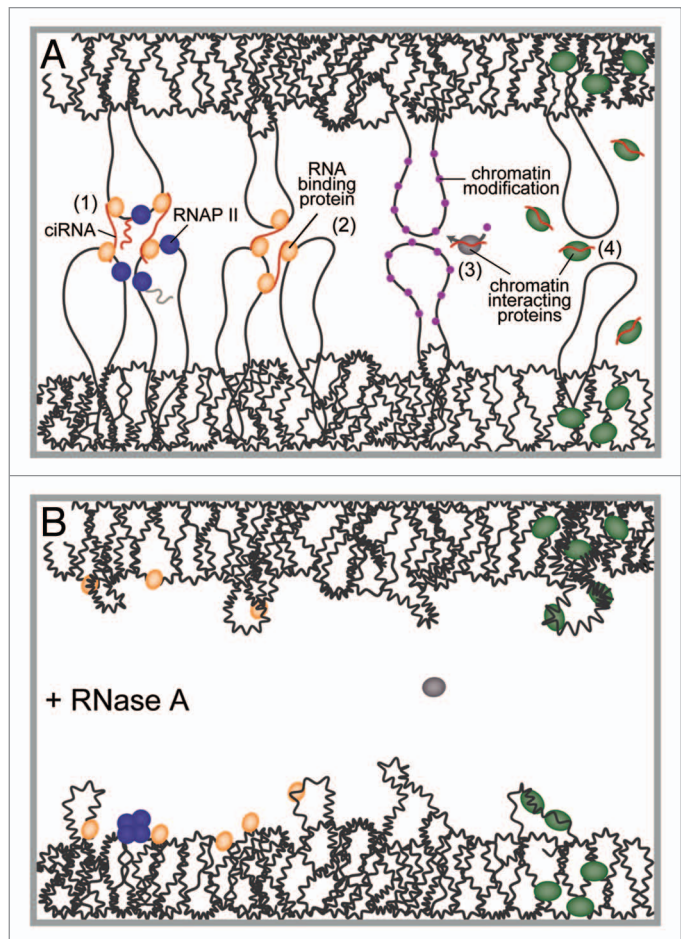


Figure 10. Hypothetical models for the role of ciRNAs as genome organizing cross-linkers. (A) (1) A network is formed between RNAP II (blue), perichromatin fibrils (black loops), nascent RNA transcripts (light gray), ciRNAs (red) and other RNA binding proteins (orange). As reported previously, RNA synthesis (and particularly ciRNAs) occurs at the surface of transcription factories around a protein-rich core.⁵⁸ (2) ciRNAs are produced by RNAP II but act in trans to create inter-chromatin links elsewhere. (3) ciRNAs act indirectly on chromatin structure by interacting with specific chromatin modifying proteins (gray) to target chromosomal modifications (purple). (4) ciRNAs interact with an unknown chromatin condensing protein (green) and inhibit its binding to chromatin, which favors the open chromatin state. (B) The degradation of ciRNAs by RNase A disrupts the open structure of chromatin in the perichromatin compartment and induces aggregation of chromatin in all four models.

rescue experiments (see below), α -amanitin was added simultaneously with RNase inhibitor 5 min before addition of the RNA fraction.

Immunofluorescence and antibodies. The anti-lamin A antibody was a gift of Dr. Harald Herrmann-Lerdon (DKFZ, Heidelberg). The anti-trimethyl-histone 3 lysine 9 (H3K9me3), the anti-RNAP II (H5) and the anti-BrdU antibodies were purchased from Millipore, GeneTex Inc., and Becton Dickinson, respectively. After PFA fixation, the cells were permeabilized for 5 min in ice cold PBS containing 0.5% Triton and washed twice in PBS. For immunofluorescence using the H5 antibody, cells were first permeabilized 1 min in 0.25% Triton prior to PFA

fixation, and then blocked for 30 min in PBS containing 10% goat serum. Incubation with the primary antibody (diluted in blocking buffer) was for 1 h at 37°C. After washing the cells first with PBS-NP40 (0.002% NP40 in PBS) and then with PBS, cells were incubated 30 min in the secondary antibody (Alexa-488 or Alexa-568 coated anti-mouse or anti-rabbit antibody, Invitrogen). Cells were stained for 5 min with a 4',6-diamidin-2'-phenylindol-dihydrochlorid (DAPI) solution (Invitrogen), washed twice in PBS and mounted overnight with mowiol (10% mowiol 4–88, 25% glycerol in 100 mM Tris pH 8.5). RNA transcripts in HeLa cells were visualized via incorporation of BrUTP (Sigma) during RNA synthesis and subsequent labeling. BrUTP was transfected 30 to 60 min with FuGENE 6 (Roche) and visualized with an anti-BrdU/BrU antibody as described previously in reference 52.

Enzymes and buffers. RNase A was obtained from Qiagen or Roche and diluted in boiled water to 14 mg/ml (1 U/ μ l). The effect of RNase A on the chromatin structure was not dependent on the buffer used in the injection mix. The buffer solutions tested were either water, 20 mM sodium phosphate buffer (pH 6.9), phosphate buffered saline (PBS), RNase H reaction buffer (50 mM Tris-HCl, pH 7.5, 100 mM NaCl, 10 mM MgCl₂), or DNase I reaction buffer (10 mM Tris-HCl, pH 7.5, 2.5 mM MgCl₂, 0.1 mM CaCl₂). RNase H, RNase III (10 U/ μ l or 100 U/ μ l and 1 U/ μ l respectively, Epicentre Biotechnologies) and RNase V1 (0.1 U/ μ l, Ambion) were provided in solution. RNases were both certified as protease- and DNase-free and tested for the absence of such activities. DNase I was from Qiagen, and dissolved in boiled DNase I buffer to a concentration of 1.5 or 15 Kunitz units per μ l. The MNase was provided in solution (50 U/ μ l, Fermentas) or lyophilized (Genaxxon Bioscience) and used at a stock concentration of 600 U/ μ l in MNase storage buffer (20 mM Tris-HCl, pH 7.6, 50 mM NaCl and 50% (v/v) glycerol). For the microinjection experiments and treatment of permeabilized cells MNase was applied in a reaction buffer containing 15 mM Hepes pH 8.0, 17 mM KCl, 4 mM NaCl and 10 mM CaCl₂. The Orn RNase was prepared as described in reference 53, and diluted to a concentration of 1 μ M or 10 μ M. Restriction enzymes *Alu* I, *Dra* I and *Hinc* II (cleaving every 250, 1,000 and 4,000 nucleotides on an average) were provided at 10 U/ μ l stocks (Fermentas). Proteinase K from Roche was diluted in PBS to concentrations of 10 μ g/ μ l or 100 μ g/ μ l.

Microinjection. Cells were grown on glass coverslips that were coated with matrigel (BD Biosciences). Each 10 μ l injection mix contained (i) 2 μ l propidium iodide (PI, 1 mg/ml, Invitrogen), which stains preferentially RNA but also DNA in case of low RNA concentrations, and was used as a re-localization marker to identify the injected cells, (ii) 1 μ l of enzyme or storage buffer for the control injection and (iii) 7 μ l of the corresponding reaction buffer. RNase A could be combined with all reaction buffers without affecting its activity. We noticed that an injection mix containing more than 5% glycerol would affect chromatin organization. Accordingly, the glycerol concentration was kept at \leq 5% glycerol in all experiments. Microinjection was performed with a computer-assisted system (AIS2, CellBiology Trading).

Injection pressure was set to 150 hPA, the injection time to 0.5 sec and the needle diameter at the output was about 300 nm. The injected volume depended on the injection pressure, injection time and capillary diameter and was 10–100 fl with the enzyme concentrations given in Table S1. We routinely injected 300 cells per sample within 20 min. During the injection process, cells were maintained in L-15 medium containing 10% FCS, 2 mM L-glutamin and 1% penicillin/streptomycin. Following the injection, cells were placed either back into cell culture medium in the incubator (37°C, 5% CO₂) for 20 min (proteinase K and RNase A samples) or 1 hour (all DNases, RNases except RNase A, and other samples) if not indicated otherwise. For fixation cells were incubated for 7 min in ice cold PBS, pH 6.8, containing 4% PFA. Fixed cells were washed two times in PBS, incubated for 5 min in a DAPI solution (Invitrogen) and mounted overnight with mowiol.

RNA extraction. RNA fractions were prepared according to the scheme in Figure 6. Total RNA was extracted from HeLa cells by guanidinisothiocyanat/phenol extraction with the Trifast kit (Peqlab). To purify nuclear and cytoplasmic RNA fractions 2 x 10⁷ HeLa cells were incubated 10 min on ice in 5 ml extraction buffer (10 mM Hepes pH 7.9, 10 mM KCl, 1.5 mM MgCl₂, 0.5 mM DTT) containing 5 μ l Ribolock RNase inhibitor (Fermentas) and transferred to a pre-cooled tissue homogenizer. Cells were dounced on ice 10 times using a tight pestle. The homogenized cells were centrifuged at 1,200 rpm (300 g) for 5 min at 4°C. The pellet contained the nuclei and the supernatant the cytoplasmic fraction. The cytoplasmic RNAs were phenol/chloroform extracted after proteinase K and DNase I treatment. The pelleted nuclei were purified by one more centrifugation step through a 12% sucrose cushion at 2,500 rpm (1,300 g) for 5 min at 4°C. The nuclear RNAs were prepared from the pelleted nuclei following the Trifast procedure. Homopolymeric poly(A) (500 to 1,500 nt in length), yeast tRNA and yeast rRNA were purchased from Amersham Biosciences, Ambion and Worthington, respectively. The soluble nuclear extract and nuclear pellet were prepared by incubating isolated nuclei in 3 ml DNase I buffer containing 3 μ l Ribolock for 10 min. The nuclei were centrifuged at 2,500 rpm (1,300 g) for 4 min at 4°C. The supernatant contained the soluble nuclear RNA extract and the pellet the nuclear pellet RNA fraction. The nuclear pellet RNA was isolated with the Trifast procedure, and the RNA from the soluble nuclear extract was phenol/chloroform extracted after proteinase K and DNase I treatment. The F1 to F4 RNA fractions were obtained from the soluble nuclear extract by loading it on a 30 ml 5–30% sucrose gradient before proteinase K and DNase I treatment. The gradient was centrifuged at 16,000 rpm (31,400 g) for 16 hours at 4°C using a Beckman SW 32 Ti swinging-bucket rotor. The respective gradient fractions (Fig. 6B) were pooled and the RNA was phenol/chloroform extracted after proteinase K and DNase I treatment. The F2 RNA fraction was depleted from polyadenylated RNAs using the Oligotex mRNA kit from Qiagen. The chromatin fraction was prepared from isolated nuclei, after DNase I digestion (1 Kunitz unit in 3 ml DNase I buffer, 37°C, 10 min) followed by incubation in 0.1 mM EDTA (30 min, 4°C) and light

sonication. The sample was then centrifuged and separated into insoluble pellet and soluble chromatin. The soluble chromatin was loaded on a sucrose gradient as described above and fractions containing DNA fragments of 1,500 to 3,000 bp (equivalent to 8 to 15 nucleosomes with a 200 bp nucleosome repeat length) were pooled. RNA was extracted by phenol/chloroform after proteinase K and DNase I treatment.

RNA rescue experiments. Cells grown on 18 mm cover slips were permeabilized for 30 s in 0.1% Triton X-100 with PBS, washed with PBS and incubated for 10 min with 700 U/ml RNase A in PBS. Cells were washed in PBS and incubated 5 min in medium supplemented with 100 μ l/ml RNase inhibitor (Ribolock, Fermentas) at 37°C, 5% CO₂. For testing the various RNA fractions, cells were incubated for 15 min after RNA addition.

Confocal fluorescence microscopy. For confocal imaging, a Leica TCS SP5 confocal laser scanning microscope (CLSM) equipped with a HCX PL APO lambda blue 63x/1.4 NA oil immersion objective was used (Leica Microsystems CMS GmbH, Mannheim, Germany). A diode-pumped solid-state laser and an Argon ion laser were used for DAPI (λ = 405 nm), Alexa 488 or GFP (λ = 488 nm) and Alexa 568 (λ = 561 nm) excitation. For the multi-color analysis, sequential image acquisition was applied and emission detection ranges were adjusted to minimize crosstalk between the different signals. The detection pinhole had a diameter corresponding to one airy disk.

Image analysis. Changes of the nuclear chromatin distribution upon treatment with RNase A were evaluated by visual inspection. All cells on a given CLSM image from an optical section were classified into two categories: “intact chromatin” and “aggregated chromatin”. To confirm that this reflected true differences in the chromatin distribution about 125 cells classified as having an intact chromatin distribution and 137 of the aggregated chromatin category were subjected to an analysis of the chromatin distribution by texture analysis via computing its fractal dimension. The approach was similar to that used previously for evaluating chromatin decondensation due to histone acetylation.²⁹ The fractal dimension was calculated for a 5 x 5 μ m square in the center of the nucleus using the ImageJ plugin MapFractalCount by Per Henden and Jens Bache-Wiig. It is based on an improved box counting method.⁵⁵ As shown in the histogram in **Figure 5B** the two groups appeared as two clearly distinct distributions in the fractal dimension analysis with an overlap of about 10%. This could be considered as the upper limit for the error associated with our classification and confirms that our visual analysis is able to reliably distinguish the differences in the chromatin compaction state.

RNA sequencing. For high-throughput sequencing, two independent preparations of each of the different RNA fractions were analyzed. For data set 1, RNAs were depleted of rRNAs using the human/mouse RiboMinus transcriptome isolation kit (Invitrogen) and for data set 2 the Ribo-Zero rRNA Removal Kit (Epicentre) was used. After rRNA depletion, RNAs were subjected to metal ion catalyzed cleavage to sizes between 60–200 nucleotides with the Ambion RNA fragmentation reagents. Libraries for Solexa sequencing were generated according to the standard

protocol for mRNA (Illumina) that comprised first strand cDNA synthesis, second strand cDNA synthesis, end repair, addition of a single A base and adapter ligation. Adapter sequences were 5'-P-GAT CGG AAG AGC TCG TAT GCC GTC TTC TGC TTG-3' and 5'-ACA CTC TTT CCC TAC ACG ACG CTC TTC CGA TC*T-3' with C* denoting a phosphorothioated cytosine. Products were amplified by PCR using the primers 5'-AAT GAT ACG GCG ACC ACC GAG ATC TAC ACT CTT TCC CTA CAC GAC GCT CTT CCG ATC*T-3' and 5'-CAA GCA GAA GAC GGC ATA CGA GCT CTT CCG ATC*T-3'. PCR products were size excised from low melting agarose gels (200–400 bp range) and phenol extracted. Sequencing was performed on the Illumina GAIIx platform at the sequencing core facilities of the EMBL, DKFZ and BioQuant in Heidelberg, Germany.

RNA sequence analysis. Initial sequence analysis was with the Bioconductor (<http://www.bioconductor.org>) package for the R statistical programming language to assess the reads quality and to produce a reads coverage file. The integrative genomics viewer (<http://www.broadinstitute.org/igv>) was used to visualize the coverage file and the RefSeq genes (NCBI). Reads were aligned with Bowtie⁵⁶ on the GRCh37/hg19 (2009) assembly version of the human genome reporting unique hits without mismatches and with and without trimming of the 3' and 5' ends. For the different RNA fractions 23–26 million reads of 36 nt length were obtained for data set 1. Between 49 to 71% of these mapped to the reference genome sequence. Ribosomal RNAs, which represented about 20% of the reads, were excluded from the analysis. For data set 2, the number of reads was between 25 and 35 million out of which 63–79% were mapped to the human genome. The ribosomal RNAs excluded from the analysis represented less than 3% of the reads of the different RNA fractions except for the chromatin sample (16% rRNAs). Peak calling was done with MACS by building a peak model to shift every read according to half the starting fragment size⁵⁷ and eventually combining overlapping peaks. Clusters were then called based on a significant enrichment in reads as compared to the local read distribution around the summit of each peak. These clusters were annotated according to RNA databases for transcription start sites (TSS), cap-associated gene expression (CAGE), promoter-associated small RNAs (pasRNAs), 3'-untranslated region (3'-UTR), small nucleolar RNAs (snoRNAs), tRNAs, micro RNAs (miRNAs), repeat-associated RNAs (rasRNAs and repeats) using the Genomatix software suite (Genomatix, Munich, Germany). After annotation, the clusters were compared to a primary transcripts (PT) database and re-grouped into PT when both exonic and intronic clusters would correspond to the same PT or spliced transcripts when only exons were found. Clusters annotated as “exon-intron overlapping” are clusters overlapping exonic and intronic regions. 3'-UTR lengths were retrieved from a 3'-UTR database (<http://www.genome.ucsc.edu/cgi-bin/hgTables>).

Sequences from the F2 RNA fraction and total RNA were analyzed with respect to their content of poly A and poly T tracts (\geq 20-mers). To determine the most enriched clusters of the F2 RNA and total RNA fractions, common clusters from the F2 RNA fraction and total RNA (2,185 clusters, data set 1 and 2,364 clusters,

data set 2) were compared based on their amount of reads. The distribution of the ratios of their reads number (for each common cluster: reads in F2 RNA fraction/reads in total RNA) was calculated. To determine the most depleted clusters of the F2 RNA fraction on one hand and the most enriched clusters of the F2 RNA fraction on the other hand, we selected the clusters corresponding to the 10% lowest and 10% highest ratios, respectively.

RNA sequence data have been submitted to the ArrayExpress database at www.ebi.ac.uk/arrayexpress under the accession number E-MTAB-582.

Disclosure of Potential Conflict of Interest

No potential conflicts of interest were disclosed.

Acknowledgments

We are grateful to Gernot Längst, Karsten Richter, Anne Seefeld, Joel Beaudouin, Nathan Brady, Undine Mechold,

Thomas Sandmann, Dirk-Peter Herten and Ingrid Grummt for help and discussions, and to Greg Hannon, Peter Lichter and Roland Eils for their support of the project, and like to thank the two reviewers of the paper for their detailed and insightful comments. Parts of the fluorescence microscopy work were conducted at the DKFZ Microscopy Core Facility and the Advanced Light Microscopy Facility at the European Molecular Biology Laboratory (Heidelberg, Germany). The project was supported by a fellowship of the Christiane Nüsslein-Volhard foundation and the “For Women in Science” program of L’Oréal-UNESCO to M.C., the SBCancer program within the Helmholtz Alliance on Systems Biology and by the BMBF funded EpiGenSys project within the EraSysBio+ program.

Note

Supplemental material can be found at:

www.landesbioscience.com/journals/nucleus/article/17773

References

- Misteli T, Soutoglou E. The emerging role of nuclear architecture in DNA repair and genome maintenance. *Nat Rev Mol Cell Biol* 2009; 10:243-54.
- Fraser P, Bickmore W. Nuclear organization of the genome and the potential for gene regulation. *Nature* 2007; 447:413-7.
- Wachsmuth M, Caudron-Herger M, Rippe K. Genome organization: Balancing stability and plasticity. *Biochim Biophys Acta* 2008; 1783:2061-79.
- Markaki Y, Gunkel M, Schermelleh L, Beichmanis S, Neumann J, Heidemann M, et al. Functional nuclear organization of transcription and DNA replication: a topographical marriage between chromatin domains and the interchromatin compartment. *Cold Spring Harbor Symp Quant Biol* 2010; 75:475-92.
- Li G, Reinberg D. Chromatin higher-order structures and gene regulation. *Curr Opin Genet Dev* 2011; 21:175-86.
- Belgrader P, Siegel AJ, Berezney R. A comprehensive study on the isolation and characterization of the HeLa S3 nuclear matrix. *J Cell Sci* 1991; 98:281-91.
- Nickerson JA, Krochmalnic G, Wan KM, Penman S. Chromatin architecture and nuclear RNA. *Proc Natl Acad Sci USA* 1989; 86:177-81.
- Pederson T. Half a century of “the nuclear matrix”. *Mol Cell Biol* 2000; 11:799-805.
- Rippe K. Dynamic organization of the cell nucleus. *Curr Opin Genet Dev* 2007; 17:373-80.
- Cook PR. A model for all genomes: the role of transcription factories. *J Mol Biol* 2010; 395:1-10.
- Chakalova L, Fraser P. Organization of Transcription. *Cold Spring Harb Perspect Biol* 2010; 2:729.
- Papantonis A, Cook PR. Genome architecture and the role of transcription. *Curr Opin Cell Biol* 2010; 22:271-6.
- Gingeras TR. Implications of chimaeric non-co-linear transcripts. *Nature* 2009; 461:206-11.
- Boisvert F, van Koningsbruggen S, Navascués J, Lamond A. The multifunctional nucleolus. *Nat Rev Mol Cell Biol* 2007; 8:574-85.
- Shopland LS, Lynch CR, Peterson KA, Thornton K, Kepper N, Hase J, et al. Folding and organization of a contiguous chromosome region according to the gene distribution pattern in primary genomic sequence. *J Cell Biol* 2006; 174:27-38.
- de Laat W, Grosveld F. Inter-chromosomal gene regulation in the mammalian cell nucleus. *Curr Opin Genet Dev* 2007; 17:456-64.
- Huang RC, Bonner J. Histone-bound RNA, a component of native nucleohistone. *Proc Natl Acad Sci USA* 1965; 54:960-7.
- Paul J, Duerksen JD. Chromatin-associated RNA content of heterochromatin and euchromatin. *Mol Cell Biochem* 1975; 9:9-16.
- Miller TE, Huang CY, Pogo AO. Rat liver nuclear skeleton and ribonucleoprotein complexes containing HnRNA. *J Cell Biol* 1978; 76:675-91.
- Ma H, Siegel A, Berezney R. Association of chromosome territories with the nuclear matrix. Disruption of human chromosome territories correlates with the release of a subset of nuclear matrix proteins. *J Cell Biol* 1999; 146:531-42.
- Rodríguez-Campos A, Azorin F. RNA is an integral component of chromatin that contributes to its structural organization. *PLoS ONE* 2007; 2:1182.
- Shevtsov SP, Dundr M. Nucleation of nuclear bodies by RNA. *Nat Cell Biol* 2011; 13:167-73.
- Wong LH, Brettingham-Moore KH, Chan L, Quach JM, Anderson MA, Northrop EL, et al. Centromere RNA is a key component for the assembly of nucleoproteins at the nucleolus and centromere. *Genome Res* 2007; 17:1146-60.
- Mondal T, Rasmussen M, Pandey GK, Isaksson A, Kanduri C. Characterization of the RNA content of chromatin. *Genome Res* 2010; 20:899-907.
- Mao YS, Sunwoo H, Zhang B, Spector DL. Direct visualization of the co-transcriptional assembly of a nuclear body by noncoding RNAs. *Nat Cell Biol* 2011; 13:95-101.
- Kapranov P, Willingham AT, Gingeras TR. Genome-wide transcription and the implications for genomic organization. *Nat Rev Genet* 2007; 8:413-23.
- Maison C, Bailly D, Peters AH, Quivy JP, Roche D, Taddei A, et al. Higher-order structure in pericentric heterochromatin involves a distinct pattern of histone modification and an RNA component. *Nat Genet* 2002; 30:329-34.
- Müller KP, Erdel F, Caudron-Herger M, Marth C, Fodor BD, Richter M, et al. Multiscale analysis of dynamics and interactions of heterochromatin protein 1 by fluorescence fluctuation microscopy. *Biophys J* 2009; 97:2876-85.
- Fejes Tóth K, Knoch TA, Wachsmuth M, Stöhr M, Frank-Stöhr M, Bacher CP, et al. Trichostatin A induced histone acetylation causes decondensation of interphase chromatin. *J Cell Sci* 2004; 117:4277-87.
- Görisch SM, Wachsmuth M, Fejes Tóth K, Lichter P, Rippe K. Histone acetylation increases chromatin accessibility. *J Cell Sci* 2005; 118:5825-34.
- Niyogi SK, Datta AK. A novel oligoribonuclease of *Escherichia coli*. I. Isolation and properties. *J Biol Chem* 1975; 250:7307-12.
- Maison C, Bailly D, Roche D, de Oca RM, Probst AV, Vassias I, et al. SUMOylation promotes de novo targeting of HP1alpha to pericentric heterochromatin. *Nat Genet* 2011; 43:220-7.
- Mignone E, Gissi C, Liuni S, Pesole G. Untranslated regions of mRNAs. *Genome Biol* 2002; 3:reviews0004.
- Chekanova JA, Belostotsky DA. Evidence that poly(A) binding protein has an evolutionarily conserved function in facilitating mRNA biogenesis and export. *RNA* 2003; 9:1476-90.
- Haaf T, Ward DC. Inhibition of RNA polymerase II transcription causes chromatin decondensation, loss of nucleolar structure and dispersion of chromosomal domains. *Exp Cell Res* 1996; 224:163-73.
- Zeng C, Kim E, Warren SL, Berget SM. Dynamic relocation of transcription and splicing factors dependent upon transcriptional activity. *EMBO J* 1997; 16:1401-12.
- Bregman DB, Du L, van der Zee S, Warren SL. Transcription-dependent redistribution of the large subunit of RNA polymerase II to discrete nuclear domains. *J Cell Biol* 1995; 129:287-98.
- Görisch SM, Wachsmuth M, Itrrich C, Bacher CP, Rippe K, Lichter P. Nuclear body movement is determined by chromatin accessibility and dynamics. *Proc Natl Acad Sci USA* 2004; 101:13221-6.
- Shav-Tal Y, Darzacq X, Shenoy SM, Fusco D, Janicki SM, Spector DL, et al. Dynamics of single mRNPs in nuclei of living cells. *Science* 2004; 304:1797-800.
- Lleres D, James J, Swift S, Norman DG, Lamond AI. Quantitative analysis of chromatin compaction in living cells using FLIM-FRET. *J Cell Biol* 2009; 187:481-96.
- Albiez H, Cremer M, Tiberi C, Vecchio L, Schermelleh L, Dittrich S, et al. Chromatin domains and the interchromatin compartment form structurally defined and functionally interacting nuclear networks. *Chromosome Res* 2006; 14:707-33.
- Richter K, Nesslering M, Lichter P. Experimental evidence for the influence of molecular crowding on nuclear architecture. *J Cell Sci* 2007; 120:1673-80.
- Rouquette J, Genoud C, Vazquez-Nin GH, Kraus B, Cremer T, Fakan S. Revealing the high-resolution three-dimensional network of chromatin and interchromatin space: a novel electron-microscopic approach to reconstructing nuclear architecture. *Chromosome Res* 2009; 17:801-10.
- Cremer T, Cremer M. Chromosome territories. *Cold Spring Harbor perspectives in biology* 2010; 2:3889.
- Bartova E, Krejci J, Harnicarova A, Galiova G, Kozubek S. Histone modifications and nuclear architecture: a review. *J Histochem Cytochem* 2008; 56:711-21.

46. Chaumeil J, Le Baccon P, Wutz A, Heard E. A novel role for Xist RNA in the formation of a repressive nuclear compartment into which genes are recruited when silenced. *Genes Dev* 2006; 20:2223-37.
47. Tsai MC, Manor O, Wan Y, Mosammaparast N, Wang JK, Lan F, et al. Long noncoding RNA as modular scaffold of histone modification complexes. *Science* 2010; 329:689-93.
48. Schmitz KM, Mayer C, Postepska A, Grummt I. Interaction of noncoding RNA with the rDNA promoter mediates recruitment of DNMT3b and silencing of rRNA genes. *Genes Dev* 2010; 24:2264-9.
49. Khalil AM, Guttman M, Huarte M, Garber M, Raj A, Rivea Morales D, et al. Many human large intergenic noncoding RNAs associate with chromatin-modifying complexes and affect gene expression. *Proc Natl Acad Sci USA* 2009; 106:11667-72.
50. Lang M, Jegou T, Chung I, Richter K, Udvarhelyi A, Münch S, et al. Three-dimensional structure of promyelocytic leukemia nuclear bodies. *J Cell Sci* 2010; 123:392-400.
51. Wolter KG, Hsu YT, Smith CL, Nechushtan A, Xi XG, Youle RJ. Movement of Bax from the cytosol to mitochondria during apoptosis. *J Cell Biol* 1997; 139:1281-92.
52. Haukenes G, Szilvay AM, Brokstad KA, Kanestrom A, Kalland KH. Labeling of RNA transcripts of eukaryotic cells in culture with BrUTP using a liposome transfection reagent (DOTAP). *Biotechniques* 1997; 22:308-12.
53. Mechold U, Ogryzko V, Ngo S, Danchin A. Oligoribonuclease is a common downstream target of lithium-induced pAp accumulation in *Escherichia coli* and human cells. *Nucleic Acids Res* 2006; 34:2364-73.
54. Mercer TR, Wilhelm D, Dinger ME, Soldà G, Korbic DJ, Glazov EA, et al. Expression of distinct RNAs from 3' untranslated regions. *Nucleic Acids Res* 2011; 39:2393-403.
55. Chen WS, Yuan SY, Hsieh CM. Two algorithms to estimate fractal dimension of gray-level images. *Opt Eng* 2003; 42:2453.
56. Langmead B, Trapnell C, Pop M, Salzberg SL. Ultrafast and memory-efficient alignment of short DNA sequences to the human genome. *Genome Biol* 2009; 10:25.
57. Zhang Y, Liu T, Meyer CA, Eickhout J, Johnson DS, Bernstein BE, et al. Model-based analysis of ChIP-Seq (MACS). *Genome Biol* 2008; 9:137.
58. Eskiw CH, Rapp A, Carter DR, Cook PR. RNA polymerase II activity is located on the surface of protein-rich transcription factories. *J Cell Sci* 2008; 121:1999-2007.

Supplementary Material

Coding RNAs with a non-coding function: maintenance of open chromatin structure

Maiwen Caudron-Herger, Katharina Müller-Ott, Jan-Philipp Mallm, Caroline Marth, Ute Schmidt, Katalin Fejes-Tóth, and Karsten Rippe

This file contains the following sections:

Supplementary Figures S1, S2 and S3

Supplementary Tables S1 and S2

Supplementary References

Supplementary Figures

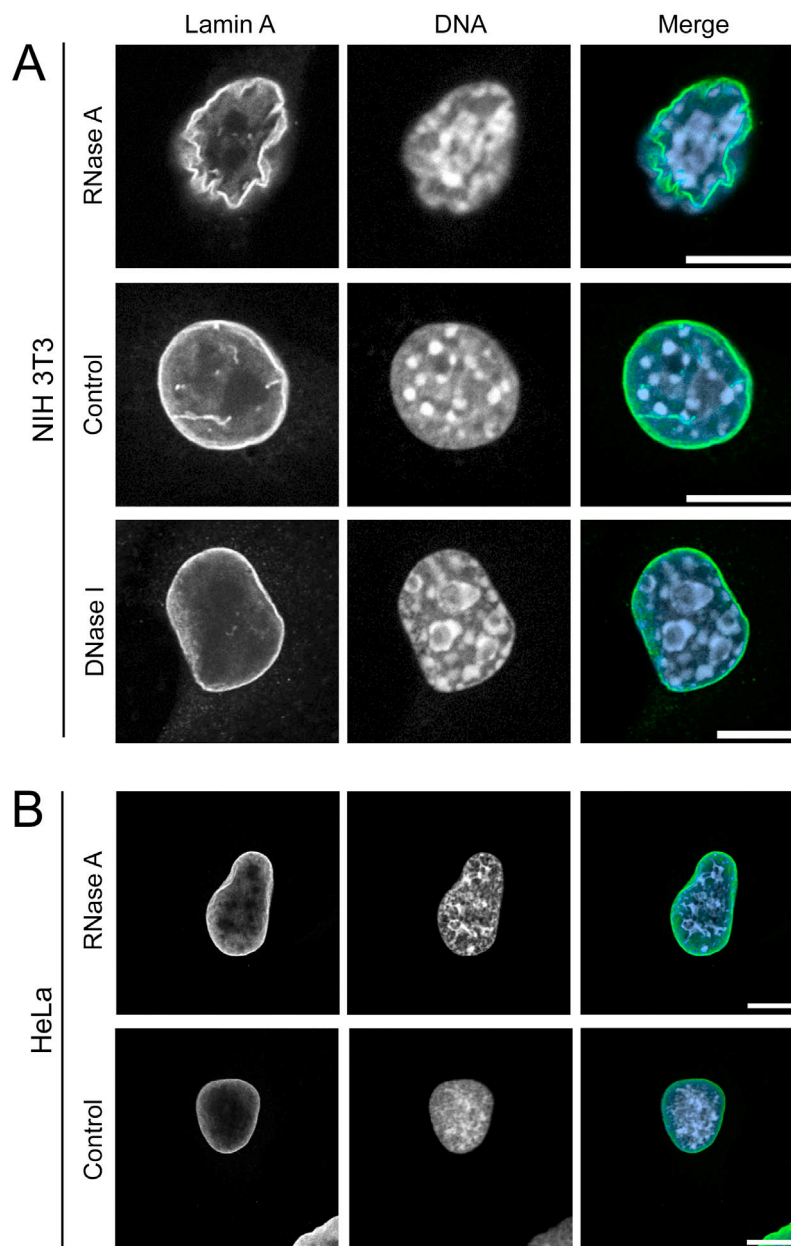


Figure S1. Immunostaining of the nuclear envelope. CLSM immunofluorescence images with an anti-lamin A antibody (green) are shown together with DAPI counterstaining of the DNA (blue). Scale bars: 10 μm . **(A)** NIH 3T3 mouse fibroblast cells. The nuclear envelope remained intact after RNase A injection but some local folding was induced. DNase I injection had no effect on the lamin A immunostaining. **(B)** The nuclear envelope of HeLa cells was unaffected by RNase A microinjection. Scale bars: 10 μm .

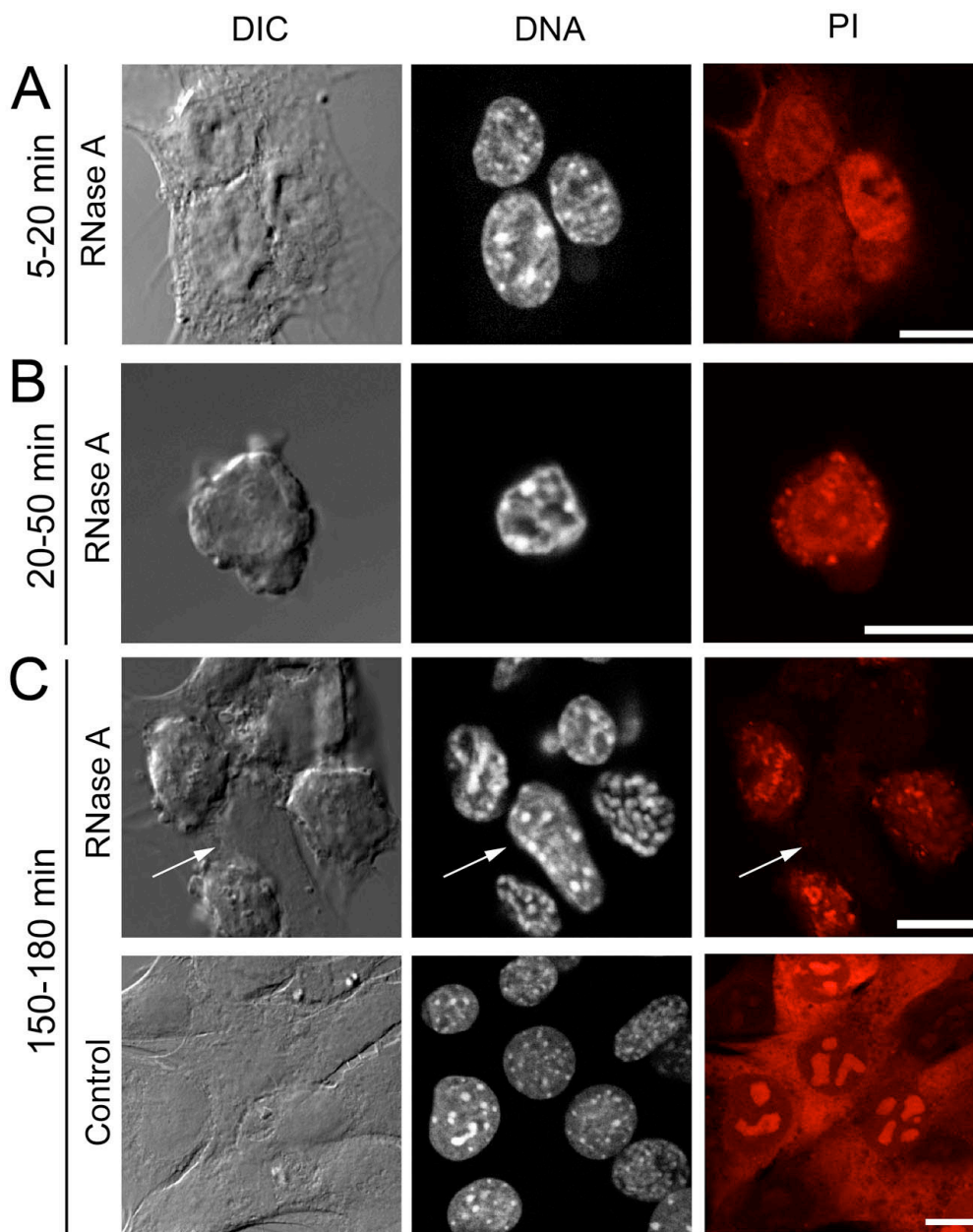


Figure S2. Time course of RNase A-induced chromatin aggregation. NIH 3T3 mouse cells were injected as indicated and fixed within **(A)** 5 to 20 min, **(B)** 20 to 50 min, and **(C)** 150 to 180 min after injection. Note that in the control sample the cells remained stably adherent to the surface like the non-injected cell in panel C (arrow, absence of PI staining). In contrast RNase A injection induced a rounding up of the cells after about 20 min as shown in panel B, and only a few cells remained attached to the glass surface after 150 min. DNA was stained with DAPI, and RNA (red) with PI. Scale bars: 10 μ m.

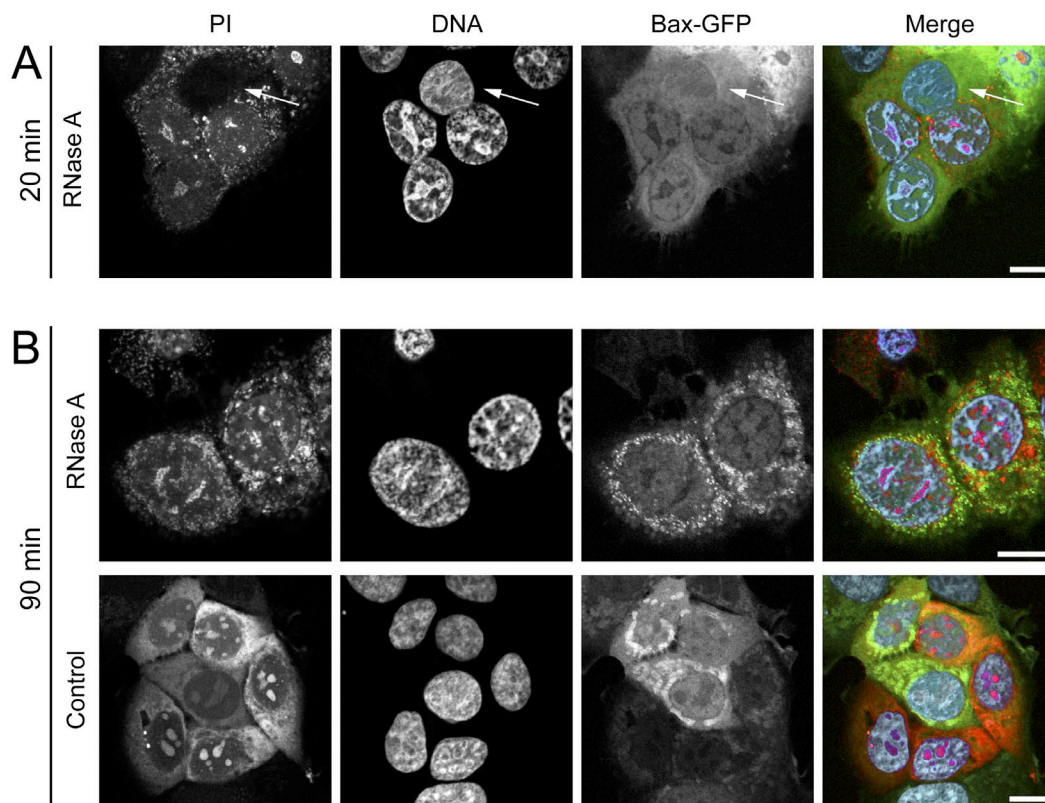


Figure S3. Time course of apoptosis induction after microinjecting RNase A into MCF-7 cells expressing Bax-GFP. Bax is a downstream effector of Bid in the caspase activation pathways via mitochondria, and can be activated also through other pathways¹⁻³. The cellular localization of Bax is a marker of induction of apoptosis. In the merged pictures, PI is in red color, Bax-GFP in green and the DAPI stained DNA is displayed in blue. Scale bars: 10 μm . **(A)** Cells fixed 20 min after RNase A injection. The MCF-7 cells expressing Bax-GFP showed the full collapse and reorganization of chromatin as observed before. Yet, both RNase A-injected cells as well as a non-injected cell (marked by an arrow) displayed a cytoplasmic distribution of Bax-GFP. Thus, apoptosis was not activated and Bax-GFP is localized in the cytosol or at the mitochondria in both injected and non-injected cells at this time point. **(B)** Cells fixed 90 min after RNase A microinjection. About half of the cells displayed a punctuated distribution of Bax-GFP, indicating the induction of the cellular events leading to apoptosis. In the RNase A sample, the apoptotic cells are identified by Bax translocation to the mitochondria, which became highly fragmented in the early stages of apoptosis. In the control cells, Bax-GFP was still localized in the cytosol or at the mitochondria.

Supplementary Tables

Table S1. Enzyme-specific effects of nucleic acid and protein digestion on chromatin structure.

Enzyme (concentration) ^a	HeLa	3T3
proteinase K (100 µg/ml)	n. d.	+
RNase A (1 U/µl)	+	+
RNase H (100 U/µl)	-	-
RNase III (1 U/µl)	-	-
RNase V1 (0.1 U/µl)	-	n. d.
DNase I (15 Ku/µl)	+	+
MNase (0.6 U/µl) ^b	+	+
Orn (10 µM)	-	-
<i>Dra</i> I (10 U/µl)	-	n. d.
<i>Hinc</i> II (10 U/µl)	-	n. d.
<i>Alu</i> I (10 U/µl)	-	-

The measured effects on the chromatin distribution were: +, large scale reorganization and aggregation of chromatin; -, no effect on chromatin structure was apparent; n. d., not determined.

^a The microinjected volume was between 10 - 100 femtoliter. For all enzymes a control injection was done with the corresponding buffer that induced no change in the chromatin distribution.

^b Enzymatic treatment via permeabilization of the cells and addition of MNase to the medium at the indicated concentration. The microinjection of MNase had no apparent effect on chromatin since sufficiently high enzyme activities could not be reached even when injecting concentrations of 60 U/µl.

Table S2. Length distribution of the 3'-UTR regions in the most enriched clusters of the F2 RNA fraction as compared to the total RNA fraction.

3'-UTR regions	Data set 1		Data set 2	
	Total RNA (%)	F2 RNA fraction (%)	Total RNA (%)	F2 RNA fraction (%)
all	41	62	21	55
> 800 nt	35	61	11	50
> 2000 nt	18	41	7	30

Supplementary References

1. Crompton M. Bax, Bid and the permeabilization of the mitochondrial outer membrane in apoptosis. *Curr Opin Cell Biol* 2000; 12:414-9.
2. Korsmeyer SJ, Wei MC, Saito M, Weiler S, Oh KJ, Schlesinger PH. Pro-apoptotic cascade activates BID, which oligomerizes BAK or BAX into pores that result in the release of cytochrome c. *Cell Death Differ* 2000; 7:1166-73.
3. Taylor RC, Cullen SP, Martin SJ. Apoptosis: controlled demolition at the cellular level. *Nat Rev Mol Cell Biol* 2008; 9:231-41.